IET Generation, Transmission & Distribution

Research Article

IET Journals
The Institution of Engineering and Technology

Contribution of FACTS devices in power systems security using MILP-based OPF

ISSN 1751-8687
Received on 5th June 2018
Accepted on 5th June 2018
doi: 10.1049/iet-gtd.2018.0376
www.ietdl.org

Ahmad Nikoobakht[1], Jamshid Aghaei[2] ✉, Masood Parvania[3], Mostafa Sahraei-Ardakani[3]

[1]*Department of Electrical Engineering, Higher Education Center of Eghlid, Eghlid, Iran*
[2]*Department of Electrical and Electronics Engineering, Shiraz University of Technology, Shiraz, Iran*
[3]*Department of Elect and Computer Engineering, University of Utah, Salt Lake City, UT 84112-9057, USA*
✉ *E-mail: aghaei@sutech.ac.ir*

Abstract: Traditionally, electric system operators have dispatched generation to minimise total production costs ignoring the flexibility of the AC transmission system (ACTS). One available option to enhance power system security is to harness the flexibility of the ACTS, where a variety of flexible AC transmission system (FACTS) devices can be incorporated in the ACTS. However, utilisation of FACTS devices is limited today due to the complexities that these devices introduce to the AC optimal power flow (ACOPF) problem. The mathematical representation of the full ACOPF problem, with the added modelling of FACTS devices, is a non-linear programming (NLP) optimisation problem, which is computationally burdensome for large-scale systems. This study presents a method to convert this NLP problem into a mixed-integer linear program (MILP) where a certain level of solution accuracy can be achieved for a time budget. In this regard, this study first proposes a linear AC OPF model, using which the OPF solution with the operation of FACTS devices is obtained. In addition, the loadability of the power systems is utilised to quantify the impacts of FACTS devices on improving the security of system. The OPF problem including FACTS devices based on a linearised model is tested on a 6-bus and the IEEE 118-bus test systems.

Nomenclature

Indices

g	index for generating units
n/m	indices for system buses
k	index for line
ℓ	index for angle piece
i/j	indices for breakpoint, the TCSC/SVC devices
s	index for load (or/and contingency state) stress condition
$(\cdot)^s$	index-related stress condition

Sets

χ_n	set of thermal units which are connected to bus n
Ω_n	set of lines which are connected to bus n
Ω_n^{SVC}	set of buses with SVCs

Continuous variables

$\delta_{nm}^{(\cdot)}$	phase angle difference across line (n, m)
$P_g^{(\cdot)}/Q_g^{(\cdot)}$	active/reactive power output of thermal unit g
$V_n^{(\cdot)}$	voltage magnitude at bus n
$P_{nm}^{(\cdot)}/Q_{nm}^{(\cdot)}$	active/reactive power flow on line (n, m)
$P_{nm}(\ell)/Q_{nm}(\ell)$	active/reactive power flow on the ℓth linear block of line (n, m)
$P_{nm}^{(\cdot)}(\ell, i)/Q_{nm}^{(\cdot)}(\ell, i)$	active/reactive power flow on the ℓth/ith linear block/breakpoint of line (n, m)
$\bar{\Delta}P_g^{(\cdot)}/\underline{\Delta}P_g^{(\cdot)}$	active power increase/decrease in thermal unit g for security purposes
Q_n^{SVC}	reactive power injected by the SVC device at bus n
B_n^{SVC}	susceptance of the SVC device at bus n
x_{nm}^{TCSC}	reactance of the TCSC device connected to line (n, m)
TC	total cost of the operation of system

Note that the normal condition $s = 0$ relates to the first stage.

Binary variables

$u_{nm}(\ell)$	status of the ℓth linear block of line (n, m)
$u_{\mathrm{tscs}}(i)/u_{\mathrm{svc}}(j)$	binary variables to represent the $x_{nm}^{\mathrm{TCSC}}/B_n^{\mathrm{SVC}}$ at the i/jth breakpoints

Constants

$\delta_{nm}^{\max}$	max angle difference across a line (n, m)
$\bar{\delta}_{nm}(\ell)$	tangent point of the ℓth piecewise linear block of angle difference across a line (n, m)
$\alpha_{nm}(\ell)/\tilde{\alpha}_{nm}(\ell)$	slope of the ℓth piecewise linear block of the linearised $F(\delta_{nm}(\ell))/\tilde{F}(\delta_{nm}(\ell))$ relative to the line (n, m) in tangent point $\bar{\delta}_{nm}(\ell)$
$\beta_{nm}(\ell)/\tilde{\beta}_{nm}(\ell)$	value of the linearised $F(\delta_{nm}(\ell))/\tilde{F}(\delta_{nm}(\ell))$ relative to the ℓth piecewise linear block of the line (n, m) in tangent point $\bar{\delta}_{nm}(\ell)$
$\alpha_{nm}(\ell, i)/\tilde{\alpha}_{nm}(\ell, i)$	slope of the ℓ/ith piecewise linear block/breakpoint of the linearised $F\big(\bar{\delta}_{nm}(\ell), g(i), b(i)\big)/\tilde{F}\big(\bar{\delta}_{nm}(\ell), g(i), b(i)\big)$ relative to the line (n, m) with TCSC device
$\beta_{nm}(\ell, i)/\tilde{\beta}_{nm}(\ell, i)$	value of the linearised $F\big(\bar{\delta}_{nm}(\ell), g(i), b(i)\big)/\tilde{F}\big(\bar{\delta}_{nm}(\ell), g(i), b(i)\big)$ relative to the ℓ/ith piecewise linear block/breakpoint of the line (n, m) with TCSC device
$\bar{b}_n/\underline{b}_n$	max/min susceptance of the SVC at bus n
$\bar{x}_k/\underline{x}_k$	max/min reactance of the TCSC at line k
C_g/C_g^s	cost of normal/stress condition of thermal unit g
$S_k^{\max}$	maximum magnitude of apparent power of line k, MVA
ψ_{D_n}	power factor angle of load n
U_g/U_k	simulated (line k)/(unit g) outage status
$\Delta R_g^{\pm}$	ramp up/down limit of thermal unit g at stress condition
$Q_g^{\max}/Q_g^{\min}$	max/min reactive power output of thermal unit g

PD_n/QD_n	active/ reactive power demand of load n
$\Delta\delta$	length of each piecewise linear block (in radians)
M	disjunctive factor, a large positive value
g_k	conductance of line k, a non-negative value
b_k/b_{k0}	series/shunt admittance of line k, a negative value
Δ_g^{LAC}	reactive power generation calculation error for LACOPF model for unit g
$\Delta_{nm}^{\mathrm{LAC}}$	reactive power flow calculation error for LACOPF model in line (n, m)
$b_n^{\mathrm{SVC}}(j)/x_{nm}^{\mathrm{TCSC}}(i)$	value of the $x_{nm}^{\mathrm{TCSC}}/B_n^{\mathrm{SVC}}$ at the i/jth breakpoints
$g_{nm}(i)/b_{nm}(i)$	value of the g_{nm}/b_{nm} at the i/jth breakpoints

1 Introduction

1.1 Motivation and aims

Today's power grids are driven closer to their transfer capacities due to the increased consumption and power transfers which results in endangering the power system security. Accordingly, maintaining the security of electric power system has increasingly become a challenging task. As a countermeasure against this issue, flexible AC transmission system (FACTS) devices have been developed [1]. FACTS devices can help reduce line flow on fully loaded transmission branches, which would lead to enhanced loadability of the power system, improved security, and eventually a further energy-efficient transmission system. Thus, this paper investigates the utilisation of FACTS devices, such as static VAR compensator (SVC) and thyristor-controlled series capacitor (TCSC), to maximise power transfer transactions during a highly stressed one that simulates a load increase under transmission line and/or thermal unit outage. Unfortunately, the FACTS device deployment are limited today due to the complexities that these devices introduce to the AC optimal power flow (ACOPF) problem. Besides, the optimal adjustment of FACTS devices introduces non-linearities in the ACOPF problem; hence, employing a non-linear solver does not guarantee to find a global optimum solution, especially when the scale of the problem is large [2]. Therefore, in order to overcome these challenges, in our paper, a linearised AC optimal power flow (LACOPF) model as well as linearised SVC and TCSC models, as target FACTS devices in this work, have been proposed.

1.2 Literature review

During the last decade, FACTS devices are broadly used for maximising the loadability of the existing power transmission networks. The possibility of operating the power system at the minimum cost whereas satisfying the network and generation constraints is one of the main issues in increasing transmission capacity by the use of FACTS [3, 4]. The FACTS devices have been effectively used in several OPF problems to reduce congestion [5], enhance security [6] and improve the voltage profile [7, 8]. It is expected that FACTS devices could increase the transfer capability over the existing transmission lines by 50% [4, 9], if deployed optimally. Major challenges that prevent better utilisation of FACTS devices in power systems are computational complexities of incorporating these devices in ACOPF problem [9–11]. In general, the ACOPF problem incorporating FACTS devices is a large-scale non-convex optimisation problem [11]. This non-convexity partly is due to the non-linearity in the active and reactive power flow equations which raise the likelihood of convergence to local optimal solutions for ACOPF problems incorporating FACTS devices [12]. There are few works in the area to address this computational challenge. For instance, the authors in [11, 13] propose various methods to include FACTS operation in OPF problem for a variety of applications. Moreover, the formulation developed in [11, 13] is computationally expensive and will not be applicable to large-scale power systems. A mixed-integer linear program (MILP)-based DC OPF model is proposed in [9, 10] to provide suggestions to the operator regarding the operation of FACTS devices and upgrading the usage of transmission capacity.

Moreover, in [9], the TCSC device has been included in the DC optimal power flow problem (DCOPF). Accordingly, the mathematical representation of the DCOPF, with the added modelling of TCSC device, is a non-linear program (NLP). This reference presents a method to convert this NLP into an MILP. It is worth mentioning that the operation of the FACTS devices based on DCOPF cannot consider ACOPF feasibility, which hinders the exploitation of the benefits of these devices, i.e. the TCSC and SVC, in power system operations.

However, the FACTS devices models based on DCOPF are unsatisfactory for the following reasons. First, the DC network model is essentially an approximation of the AC model by relaxing the reactive power and voltage constraints. These relaxations tend to create a 'gap' between the solutions obtained from the DC model and the AC model. In some cases, the gap could be large and result in an OPF solution that is problematic in the AC network. Also, because the DC model's solutions cannot consider AC feasibility, system security might be jeopardised when implementing the FACTS devices [7, 11]. Second, the inaccuracy of the DCOPF may lead to model solutions, with the TCSC and/or SVC devices, that underestimate security cost savings or, worse yet, security cost increases [1, 12, 14]. Third, the FACTS devices model based on DCOPF cannot be used to grasp other potential benefits of FACTS devices action, such as correcting temporary voltage violations [7]. Also, in the previous works mentioned above, the linear programming approach has been used based on the linearised power flow that provides only the active power of the network. The use of only active power in the OPF model with the FACTS devices action causes enormous error in power system studies, especially for SVC device where the voltage magnitude plays a critical role [9, 10]. Also, maximising the loadability and minimising security cost of an AC power system are directly related to the reactive power sufficiency and voltage security in AC network which are relaxed in DCOPF model [11]. These drawbacks suggest that the development of FACTS devices based on the AC network security constraints is of great significance and motivate the research described in this paper.

In some papers, the Newton–Raphson method has been used [15, 16]; however, this method depends essentially on the initial conditions and has difficulties in handling inequality constraints. In addition, many heuristic methods, such as genetic algorithm [4], particle swarm optimisation [17], Tabu search [18], artificial bee colony [19] among the others, were successfully applied to the OPF problem incorporating FACTS devices. However, these heuristic methods do not guarantee to obtain the global optimum solution and consequently, they are not effective methods to solve the above-mentioned problem, particularly once the scale of the power system is large. Also, the linearisation process in this paper, for the linearised AC model and TCSC and SVC device models, involves many techniques including Taylor series expansion theory, binary expansion discretisation approach, piecewise linear (PWL) approximation, and other simple techniques [12]. The proposed linearisation method has many applications in power system problems such as a unified power flow controller (or UPFC) device, static synchronous compensator (STATCOM), and a static synchronous series compensator (SSSC) [6]. Also, the UPFC device is a combination of a STATCOM and an SSSC coupled via a common DC voltage link. It might be necessary to employ further linearisation methods in order to apply the presented work to these devices [17]. The main advantage of the UPFC is to control the active and reactive power flows in the transmission line. The controllable parameters of the UPFC are reactance in the line, phase angle, and voltage. Since the presented work considers both reactive power and voltage, the linear UPFC device model can be implemented in the proposed OPF model. However, it should be highlighted that in an optimisation problem for the OPF problem, bus voltage magnitudes may differ more significantly from 1 p.u. which can affect the accuracy of the proposed method to implement the linear UPFC, STATCOM, and SSSC devices' models. Hence, to assess the preciseness, feasibility, and

applicability of the proposed method to this area, many numerical studies have to be done.

Table 1 shows the taxonomy of the proposed LACOPF model incorporating linear FACTS (LFACTS) devices model, namely TSCS and SVC, in previous literatures.

1.3 Contributions

Considering the above literature review, which summarised the existing literature and identified the state-of-the-art challenges, the novelty of this work are twofold:

i. The paper develops a linearised AC model incorporating linearised FACTS devices model, such as SVC and TCSC, in which bus voltage magnitudes and reactive power are taken into account. Based on this linearised AC model, a novel OPF formulation with LFACTS devices is proposed.
ii. The proposed method enables the utilisation of FACTS devices (such as TCSC and SVC) based on the LAC power flow model, to enhance the system security under stressed loading conditions and system contingencies.

To the best of the authors' knowledge, no reference has provided the MILP formulation for ACOPF model with linearised FACTS devices model (i.e. TCSC and SVC models), in the presence of the stressed loading condition under contingency state.

2 Linearisation of the full AC power flow with FACTS devices model

This section presents a linear approximation to AC power flow in which voltage and reactive power are modelled. The linearisation process in this section, for the linearised AC power flow model and TCSC and SVC device models, involves many techniques including Taylor series expansion theory, binary expansion discretisation approach, PWL approximation, and other simple techniques [12]. Furthermore, the linearisation process in this paper for the following assumptions is assumed to be valid:

i. The phase difference between the voltages at both ends of every existing or constructed lines is small enough, i.e. $\delta_{nm} \simeq 0 - 34^{\circ}$. This implies validation of PWL approximation of sine and cosine functions in $\underline{\delta}_{nm} < \delta_{nm} < \bar{\delta}_{nm}$. Also, at $\delta_{nm} = 34^{\circ}$, the difference between $\sin\delta_{nm}$ and δ_{nm} is 2.43%, so the fourth assumption ($\sin\delta_{nm} \simeq \delta_{nm}$) is quite reasonable.
ii. The voltage magnitudes are nearly 1 p.u. for all buses. These assumptions are practically true for large-scale systems, maintaining the system far from instability and other security limits.

2.1 Linearisation of the AC power flow equations

If the phase shifters and off-nominal transformer turns ratios are ignored, the active and reactive AC power flow in transmission line k between buses n and m is written as follows:

$$P_{nm} = g_k V_n^2 - V_n V_m \overbrace{(g_k \cos\delta_{nm} + b_k \sin\delta_{nm})}^{F(\delta_{nm})} \tag{1a}$$

$$Q_{nm} = -(b_k + b_{k0})V_n^2 + V_n V_m \overbrace{(b_k \cos\delta_{nm} - g_k \sin\delta_{nm})}^{\tilde{F}(\delta_{nm})} \tag{1b}$$

where $F(\delta_{nm})$ and $\tilde{F}(\delta_{nm})$ are non-linear functions. Assume, also they have local convexity within the specific interval, e.g. $\underline{\delta}_{nm} < \delta_{nm} < \bar{\delta}_{nm}$. One can represent $F(\delta_{nm})$ and $\tilde{F}(\delta_{nm})$ using PWL functions as did in [21], with $2L$-pieces (as shown in Fig. 1). It is noted that the illustrated curves in Figs. 1*a* and *b* show the typical form of functions $\tilde{F}(\delta_{nm})$ and $F(\delta_{nm})$ based on the real values of b_k and g_k in the real transmission networks. The convex approximation of the $F(\delta_{nm})$ and $\tilde{F}(\delta_{nm})$ functions are implemented through a PWL function that produces a linear formulation in the following way. As shown in Fig. 1, the linear approximation of the $F(\delta_{nm})$ and $\tilde{F}(\delta_{nm})$ in the range of $[-L, L]$ can be obtained using $2L$-piece PWL approximation. Accordingly, ℓth piece function for each line (n, m) through the tangent point (i.e. $\bar{\delta}_{nm}(\ell)$) is obtained as follows:

$$\begin{aligned} F(\delta_{nm}) &= \alpha_{nm}(\ell)\big(\delta_{nm} - \bar{\delta}_{nm}(\ell)\big) + \beta_{nm}(\ell), \\ &\forall \delta_{nm} \in [(-L-1+\ell)\Delta\delta,\ (-L+\ell)\Delta\delta],\ \ell = 1, \ldots, 2L \end{aligned} \tag{1c}$$

$$\begin{aligned} \tilde{F}(\delta_{nm}) &= \tilde{\alpha}_{nm}(\ell)\big(\delta_{nm} - \bar{\delta}_{nm}(\ell)\big) + \tilde{\beta}_{nm}(\ell), \\ &\forall \delta_{nm} \in [(-L-1+\ell)\Delta\delta,\ (-L+\ell)\Delta\delta],\ \ell = 1, \ldots, 2L \end{aligned} \tag{1d}$$

where $\alpha_{nm}(\ell)$ and $\tilde{\alpha}_{nm}(\ell)$ are the slope of each linear piece, at tangent point (i.e. $\bar{\delta}_{nm}(\ell)$), for the $F(\delta_{nm})$ and $\tilde{F}(\delta_{nm})$, respectively. Besides, $\beta_{nm}(\ell)$ and $\tilde{\beta}_{nm}(\ell)$ are the values of the $F(\delta_{nm})$ and $\tilde{F}(\delta_{nm})$ at the tangent point (i.e. $\bar{\delta}_{nm}(\ell)$) for each linear piece, respectively. Note that, the execution of (1c) and (1d) for the PWL model of $F(\delta_{nm})$ and $\tilde{F}(\delta_{nm})$ requires either binary variables or special ordered sets of type 2 (SOS-2) [22]. Finally, the parameters $\alpha_{nm}(\ell)$, $\tilde{\alpha}_{nm}(\ell)$, $\beta_{nm}(\ell)$, and $\tilde{\beta}_{nm}(\ell)$ are obtained by the below equations:

$$\alpha_{nm}(\ell) = \frac{\partial \tilde{F}}{\partial \delta_{nm}}\big(\delta_{nm} = \bar{\delta}_{nm}(\ell)\big),\ \tilde{\alpha}_{nm}(\ell) = \frac{\partial \tilde{F}}{\partial \delta_{nm}}\big(\delta_{nm} = \bar{\delta}_{nm}(\ell)\big) \tag{1e}$$

$$\beta_{nm}(\ell) = F\big(\delta_{nm} = \bar{\delta}_{nm}(\ell)\big) \text{ and } \tilde{\beta}_{nm}(\ell) = \tilde{F}\big(\delta_{nm} = \bar{\delta}_{nm}(\ell)\big) \tag{1f}$$

where

$$\bar{\delta}_{nm}(\ell) = \frac{(-L-1+\ell)\Delta\delta + (-L+\ell)\Delta\delta}{2}$$

Substituting (1c) and (1d) into (1a) and (1b), then we obtain the following equations: (see (1g))

Table 1 Taxonomy of our proposed model in current paper (CP)

Refs	Year	LACOPF (MILP)	LFACTS devices (MILP)		Security enhancement through a stressed conditions		
			TCSC	SVC	Load condition	Unit outage	Line outage
[9]	2016	N	Y	N	N	N	N
[12]	2016	Y	N	N	N	N	N
[13]	2014	N	N	N	N	N	N
[11]	2008	N	N	N	Y	N	Y
[8]	2013	N	N	N	Y	N	N
[20]	2015	N	N	N	N	N	N
[10]	2016	N	Y	N	N	N	N
[4]	2012	N	N	N	N	N	N
current paper		Y	Y	Y	Y	Y	Y

Y/N denote that the subject is/is not considered.

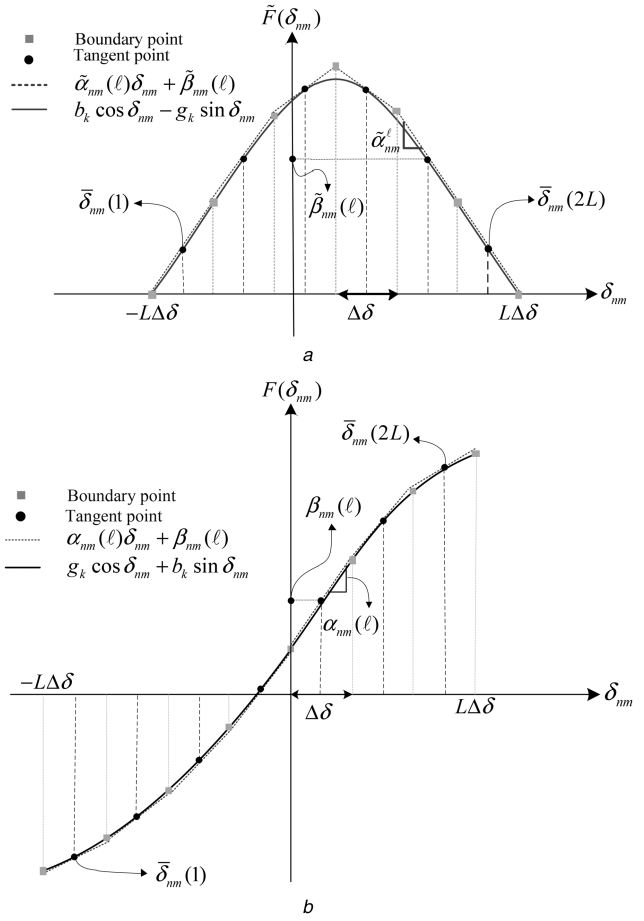

Fig. 1 *The illustration of linearisation of AC OPF formulation*
(a) Piecewise-linear approximation of $\tilde{F}(\delta_{nm})$ using $2L$-piece equalities, ***(b)*** Piecewise-linear approximation of $F(\delta_{nm})$ using $2L$-piece equalities

Table 2 Approximation errors in line flow terms (voltages and angle in p.u. and radian, respectively)

Term	Range of operation	Approximation	Max abs error
V_n^2	$0.95 \le V_n \le 1.05$	$2V_n - 1$	0.0025
V_nV_m	$0.95 \le V_{n/m} \le 1.05$	$V_n + V_m - 1$	0.0025
$V_nV_m\delta_{nm}$	$0.95 \le V_{n/m} \le 1.05$ and $\delta_{nm} \approx \bar{\delta}_{nm}(\ell)$	$\bar{\delta}_{nm}(\ell)(V_n + V_m - 1) + (\delta_{nm} - \bar{\delta}_{nm}(\ell))$	0.0050

$$\begin{aligned} Q_{nm}(\ell) &\simeq -(b_k + b_{k0})V_n^2 + V_nV_m\left[\tilde{\alpha}^{\ell}_{nm}\left(\delta_{nm} - \bar{\delta}_{nm}(\ell)\right) + \tilde{\beta}_{nm}(\ell)\right] \\ &= -(b_k + b_{k0})V_n^2 + V_nV_m\tilde{\alpha}_{nm}(\ell)\delta_{nm} \\ &\quad - V_nV_m\tilde{\alpha}_{nm}(\ell)\bar{\delta}_{nm}(\ell) + V_nV_m\tilde{\beta}_{nm}(\ell) \end{aligned} \tag{1h}$$

Notice that (1g) and (1h) still contain some non-linear terms like V_nV_m, $V_nV_m\delta_{nm}$, and V_n^2. These non-linear terms can be linearised by their Taylor series expansion around 1, for bus voltage, and about $\bar{\delta}_{nm}(\ell)$, for line angle, as presented in Table 2.

Table 2 gives the maximum absolute errors for each of the constituent terms with respect to the linearised forms, over a typical range of operating voltages and angles, i.e. $0.95 \le V_n \le 1.05$ at the end of each line, and $|\delta_{nm}| \le 34^{\circ}$. The maximum absolute errors for each of the linearised term in Table 2, over a maximum range of operating voltages and angles, i.e. $V_n^{\max} = 1.05$, $\bar{\delta}^{\max}_{nm}(\ell) = 10^{\circ}$, and $\delta_{nm} = 10 - 15^{\circ}$, are obtained from:

i. $\left|(V_n^{\max})^2 - (2V_n^{\max} - 1)\right| \simeq 0.0025$,
ii. $|V_n^{\max}V_m^{\max} - (V_n^{\max} + V_m^{\max} - 1)| \simeq 0.0025$,
iii. $\left|V_n^{\max}V_m^{\max}\delta^{\max}_{nm} - \left(\bar{\delta}^{\max}_{nm}(\ell)(V_n^{\max} + V_m^{\max} - 1) + (\delta^{\max}_{nm} - \bar{\delta}^{\max}_{nm}(\ell))\right)\right|$. $\simeq 0.0050$

Subsequently, the PWL approximation of active and reactive AC power flow equations for line (n, m) metered at bus n for the ℓth angle piece (or through the tangent point, i.e. $\bar{\delta}_{nm}(\ell)$) are obtained as follows, respectively:

$$\begin{aligned} P_{nm}(\ell) = g_k(2V_n - 1) - \alpha_{nm}(\ell)\left[\delta_{nm} - \bar{\delta}_{nm}(\ell)\right] \\ -\beta_{nm}(\ell)(V_n + V_m - 1) \end{aligned} \tag{1i}$$

$$\begin{aligned} Q_{nm}(\ell) = -(b_k + b_{k0})(2V_n - 1) + \tilde{\alpha}_{nm}(\ell)\left[\delta_{nm} - \bar{\delta}_{nm}(\ell)\right] \\ +\tilde{\beta}_{nm}(\ell)(V_n + V_m - 1) \end{aligned} \tag{1j}$$

2.2 Linearisation of TCSC equations

The model of the TCSC device used in this paper is a variable reactance connected in series with a transmission line [23]. The main idea behind power flow control with the TCSC device is to change the whole transmission line's effective series impedance, by adding inductive or capacitive impedance. That is

$$z_k = r_k + \mathrm{j}(x_k + x_{\mathrm{TCSC}}) = \frac{1}{g_k + \mathrm{j}b_k}, \quad k \in (n, m) \tag{2a}$$

The resulting conductance and susceptance are as follows, respectively:

$$g_{nm} = \frac{r_{nm}}{r_{nm}^2 + \left(x_{nm} + x_{nm}^{\mathrm{TCSC}}\right)^2}, \quad x_{nm}^{\mathrm{TCSC}} \in [\underline{x}_k, \bar{x}_k] \tag{2b}$$

$$b_{nm} = \frac{-\left(x_{nm} + x_{nm}^{\mathrm{TCSC}}\right)}{r_{nm}^2 + \left(x_{nm} + x_{nm}^{\mathrm{TCSC}}\right)^2}, \quad x_{nm}^{\mathrm{TCSC}} \in [\underline{x}_k, \bar{x}_k] \tag{2c}$$

Notice that (2b) and (2c) are non-linear terms and they need to be piecewisely linearised. One way is to represent g_{nm} and b_{nm} using the PWL functions, with I-pieces (as shown in Fig. 2).

It is noted that the demonstrated curves in Fig. 2*a* show the typical form of g_{nm} and b_{nm} terms as functions of the real values of x_{nm}^{TCSC}. The convex approximation of these non-linear terms is implemented through PWL blocks that produce a linear formulation in the following way. As shown in Fig. 2, the linear approximation of these non-linear terms in the range of $[\underline{x}_k, \bar{x}_k]$ can be obtained using I-piece PWL approximation, i.e. $x_{nm}^{\mathrm{TCSC}}(i) = \underline{x}_k + i \cdot (\bar{x}_k - \underline{x}_k)/I, \quad i = 0, 1, 2, \ldots, I$. Accordingly, the ith piece function for each g_{nm} and b_{nm} at the ith breakpoint is obtained as follows:

$$g_{nm}(i) = \frac{r_{nm}}{r_{nm}^2 + \left[x_{nm} + x_{nm}^{\mathrm{TCSC}}(i)\right]^2}, \quad i = 0, 1, 2, \ldots, I \tag{2d}$$

$$b_{nm}(i) = \frac{-\left[x_{nm} + x_{nm}^{\mathrm{TCSC}}(i)\right]}{r_{nm}^2 + \left[x_{nm} + x_{nm}^{\mathrm{TCSC}}(i)\right]^2}, \quad i = 0, 1, 2, \ldots, I \tag{2e}$$

$$\begin{aligned} P_{nm}(\ell) &\simeq g_kV_n^2 - V_nV_m\left[\alpha_{nm}(\ell)\left(\delta_{nm} - \bar{\delta}_{nm}(\ell)\right) + \beta_{nm}(\ell)\right] \\ &= g_kV_n^2 - V_nV_m\alpha_{nm}(\ell)\delta_{nm} + V_nV_m\alpha_{nm}(\ell)\bar{\delta}_{nm}(\ell) - V_nV_m\beta_{nm}(\ell) \end{aligned} \tag{1g}$$

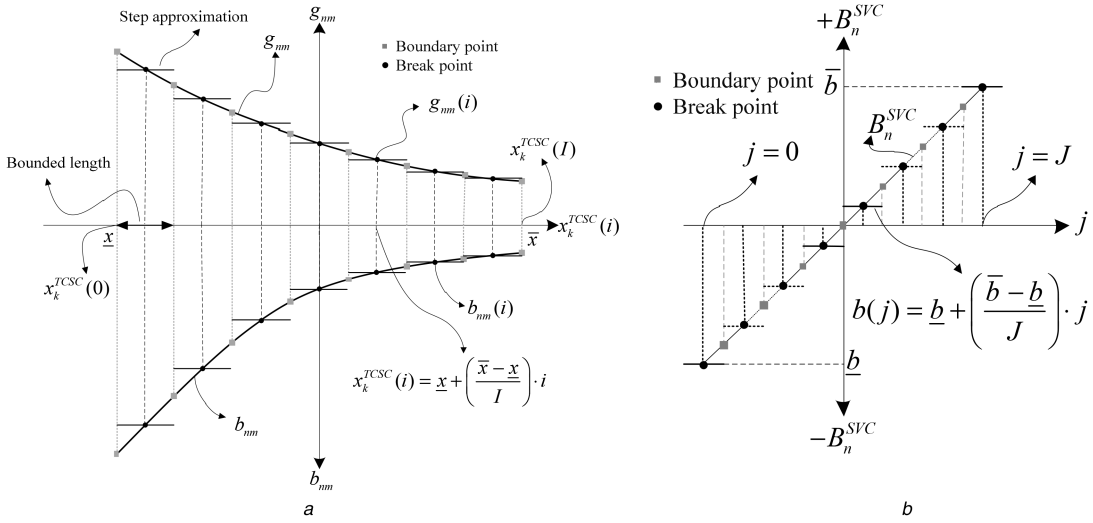

Fig. 2 *Piecewise linearisation of:*
(a) g_{nm} and b_{nm} for TCSC, and ***(b)*** B_n^{SVC} for SVC model

where $g_{nm}(i)$ and $b_{nm}(i)$ are chosen such that the approximation coincides with g_{nm} and b_{nm} at breakpoints $\left\{x_{nm}^{\mathrm{TCSC}}(0), x_{nm}^{\mathrm{TCSC}}(1), \ldots, x_{nm}^{\mathrm{TCSC}}(I)\right\}$.

Accordingly, the power flow equations of the lines with TCSC can be written as follows:

$$P_{nm}(\ell, i) = g_k(i)(2V_n - 1) - \alpha_{nm}(\ell, i)\left[\delta_{nm} - \bar{\delta}_{nm}(\ell)\right] - \beta_{nm}(\ell, i)(V_n + V_m - 1) \tag{2f}$$

$$Q_{nm}(\ell, i) = -[b_k(i) + b_{k0}](2V_n - 1) + \tilde{\alpha}_{nm}(\ell, i)\left[\delta_{nm} - \bar{\delta}_{nm}(\ell)\right] + \tilde{\beta}_{nm}(\ell, i)(V_n + V_m - 1) \tag{2g}$$

Equations (2f) and (2g) are modelled similar to that of (1i)–(1j). The main difference between (2f) and (2g) and (1i) and (1j) is that the $g_k(i)$, $\alpha_{nm}(\ell, i)/\tilde{\alpha}_{nm}(\ell, i)$, and $\beta_{nm}(\ell, i)/\tilde{\beta}_{nm}(\ell, i)$ will be specified at the ith breakpoint. The active and reactive power flow in a line with TCSC device for each of the ℓth piece then can be reformulated in the form of MILP (M is a large number) as follows:

$$P_{nm}^{\mathrm{TCSC}}(\ell, i) - M[1 - u_{\mathrm{TCSC}}(i)] \le P_{nm}(\ell) \le P_{nm}^{\mathrm{TCSC}}(\ell, i) + M[1 - u_{\mathrm{TCSC}}(i)] \tag{2h}$$

$$Q_{nm}^{\mathrm{TCSC}}(\ell, i) - M[1 - u_{\mathrm{TCSC}}(i)] \le Q_{nm}(\ell) \le Q_{nm}^{\mathrm{TCSC}}(\ell, i) + M[1 - u_{\mathrm{TCSC}}(i)] \tag{2i}$$

Constraints (2h) and (2i) are calculated at one of the breakpoints, i.e. $x_{nm}^{\mathrm{TCSC}}(0), x_{nm}^{\mathrm{TCSC}}(1), \ldots, x_{nm}^{\mathrm{TCSC}}(I)$, for a line with TCSC device at each of the ℓ th piece. Here, $u_{\mathrm{TCSC}}(i)$ is a binary variable to select one of $x_{nm}^{\mathrm{TCSC}}(0), x_{nm}^{\mathrm{TCSC}}(1), \ldots, x_{nm}^{\mathrm{TCSC}}(I)$, and M is a sufficiently large positive scalar.

Equations (2j)–(2m) are modelled similar to that of (1c)–(1f). The main difference between these equations and (1c)–(1f) are the existence of the $g(i)$ and $b(i)$ in these equations, which are dependent on the ith piece

$$F\left(\bar{\delta}_{nm}(\ell), g(i), b(i)\right) = \alpha_{nm}(\ell, i)\left(\delta_{nm} - \bar{\delta}_{nm}(\ell)\right) + \beta_{nm}(\ell, i) \quad \forall \delta_{nm} \in [(-L - 1 + \ell)\Delta\delta, (-L + \ell)\Delta\delta],\ \ell = 1, \ldots, 2L \tag{2j}$$

$$\tilde{F}\left(\bar{\delta}_{nm}(\ell), g(i), b(i)\right) = \tilde{\alpha}_{nm}(\ell, i)\left(\delta_{nm} - \bar{\delta}_{nm}(\ell)\right) + \tilde{\beta}_{nm}(\ell, i) \quad \forall \delta_{nm} \in [(-L - 1 + \ell)\Delta\delta, (-L + \ell)\Delta\delta],\ \ell = 1, \ldots, 2L \tag{2k}$$

$$\alpha_{nm}(\ell, i) = \frac{\partial F^{\ell}}{\partial \delta_{nm}}\left(\bar{\delta}_{nm}(\ell), g(i), b(i)\right) \quad \text{and} \quad \tilde{\alpha}_{nm}(\ell, i) = \frac{\partial \tilde{F}^{\ell}}{\partial \delta_{nm}}\left(\bar{\delta}_{nm}(\ell), g(i), b(i)\right) \tag{2l}$$

$$\beta_{nm}(\ell, i) = F\left(\bar{\delta}_{nm}(\ell), g(i), b(i)\right) \quad \text{and} \quad \tilde{\beta}_{nm}(\ell, i) = \tilde{F}\left(\bar{\delta}_{nm}(\ell), g(i), b(i)\right) \tag{2m}$$

The above-mentioned formulations, i.e. (1) and (2), are valid for each segment of the δ_{nm} (where $(-L - 1 + \ell)\Delta\delta < \delta_{nm} < (-L + \ell)\Delta\delta$, $\ell \in [-L, L]$), or close to each tangent point (i.e. $\bar{\delta}_{nm}(\ell)$), as shown in Fig. 1. Note that the length of each segment of angle is $\Delta\delta$ (as shown in Fig. 1). More details about piecewise linearisation can be found in [21]. It essentially introduces $2L$ new binary variables and $2L$ new inequalities, all being linear. To ensure which segment of the PWL blocks is selected, a binary variable $u_{nm}(\ell)$ is used as follows:

$$(-L - 1 + \ell)\Delta\delta - M(1 - u_{nm}(\ell)) < \delta_{nm} < (-L + \ell)\Delta\delta + M(1 - u_{nm}(\ell)) \tag{2n}$$

$$\sum_{\ell} u_{nm}(\ell) = 1 \tag{2o}$$

Note that, each angle difference across a line (n, m) metered at bus n only can be placed on one linear piece as done by (2o), where, the active or reactive line flows for line (n, m) metered at bus n are obtained as follows:

$$P_{nm}(\ell) - M(1 - u_{nm}(\ell)) \le P_{nm} \le P_{nm}(\ell) + M(1 - u_{nm}(\ell)), \quad k \in (n, m) \tag{2p}$$

$$Q_{nm}(\ell) - M(1 - u_{nm}(\ell)) \le Q_{nm} \le Q_{nm}(\ell) + M(1 - u_{nm}(\ell)), \quad k \in (n, m) \tag{2q}$$

Here, $u_{nm}(\ell)$ is a binary variable, and M a sufficiently large positive scalar. However, adding the binary variables (especially, in constraint (2p)) is likely to complicate the resultant model and makes it inefficient once the problem is implemented for a large-scale system. For this reason, if (1i) approximated with one block angle at zero tangent point (i.e. $\bar{\delta}_{nm}(\ell) = 0$), then (1i) becomes a convex equation and no binary variable is needed. Accordingly, constraint (2p) could be removed from the problem. In addition, by this action, the proposed model can be relaxed, which is named relaxed method (RM) approach, to make trade-off between the model accuracy and the computation time.

2.3 Linearisation of the SVC equations

The SVC device is a variable shunt susceptance that may have two modes: inductive or capacitive [24]. Hence, the reactive power injected by the SVC device at bus n is:

$$Q_n^{\mathrm{SVC}} = -B_n^{\mathrm{SVC}} V_n^2, \quad n \in \Omega_n^{\mathrm{SVC}} \tag{3a}$$

$$\underline{b}_n \le B_n^{\mathrm{SVC}} \le \bar{b}_n, \quad n \in \Omega_n^{\mathrm{SVC}} \tag{3b}$$

Notice that (3a) is non-convex and non-linear owing to the multiplication of variables like V_n^2 and B_n^{SVC}, thus, it is needed to be piecewisely linearised. Non-linear term of V_n^2 in this equation can be linearised by linear approximation as presented in Table 2. Moreover, as shown in Fig. 2*b*, the continuous variable B_n^{SVC} can be represented by j pieces, i.e. multiplication of parameter $b_n^{\mathrm{SVC}}(j)$ and binary variable $u_{\mathrm{SVC}}(j)$ represent the B_n^{SVC}, which is denoted by the below equations

$$B_n^{\mathrm{SVC}} = u_{\mathrm{SVC}}(0)\cdot b(0) + u_{\mathrm{SVC}}(1)\cdot b(1) + \cdots + u_{\mathrm{SVC}}(J)\cdot b(J), \quad j = 0, 1, \ldots, J \tag{3c}$$

$$b(j) = \underline{b}_n + \left(\frac{\bar{b}_n - \underline{b}_n}{J}\right)\cdot j, \quad j = 0, 1, \ldots, J \tag{3d}$$

In (3c), the B_n^{SVC} is expressed as one linear piece of $b_n^{\mathrm{SVC}}(j)$ and this linear piece is specified by a binary variable, i.e. $u_{\mathrm{SVC}}(j)$. Also, the value of parameter $b(j)$ is specified by (3d) for index j. Constraint (3e) guarantees that just one linear piece (i.e. one parameter value of $b_n^{\mathrm{SVC}}(j)$) is selected by binary variable $u_{\mathrm{SVC}}(j)$. For instance, if the first piece is selected, i.e. $u_{\mathrm{svc}}(1) = 1$, then $u_{\mathrm{SVC}}(j) = 0, \quad \forall j \ne 1$. Accordingly, we have

$$\sum_j u_{\mathrm{SVC}}(j) \le 1 \tag{3e}$$

Substituting (3c) and linear approximation of V_n^2 (i.e. $2V_n - 1$), into (3a) then (3f) is obtained as

$$Q_n^{\mathrm{SVC}} = -(2V_n - 1)\cdot \sum_j \left[u(j)\cdot b_n^{\mathrm{SVC}}(j)\right], \quad n \in \Omega_n^{\mathrm{SVC}} \tag{3f}$$

Nevertheless, (3f) still is a non-linear equation, because it includes the multiplication of $[u(j)\cdot b_n^{\mathrm{SVC}}(j)]$ and $(2V_n - 1)$ terms. Thus, the subsequent ACOPF becomes an MINLP. However, this equation can be rewritten as a disjunctive linear constraint to avoid the non-linearity without loss of generality as follows:

$$-b_n^{\mathrm{SVC}}(j)(2V_n - 1) - M(1 - u_{\mathrm{svc}}(j)) \le Q_n^{\mathrm{SVC}} \le -b_n^{\mathrm{SVC}}(j)(2V_n - 1) + M(1 - u_{\mathrm{svc}}(j)), \quad n \in \Omega_n^{\mathrm{SVC}} \tag{3g}$$

3 Model description

This section describes in detail all constraints used in the proposed LACOPF problem incorporating linearised FACTS model. Accordingly, the proposed formulation for LACOPF is addressed in the following subsections by (4) and (5). In these formulations, the total cost (TC) of the system is considered as the objective function as mentioned in (4a), which is subjected to the first- and second-stage constraints, (4) and (5), respectively

$$\min \ \mathrm{TC} = \sum_g \left(C_g P_g^0 + C_g^s\left(\underline{\Delta} P_g^s + \bar{\Delta} P_g^s\right)\right) \tag{4a}$$

The objective function consists of two main parts: first-stage and second-stage parts. The first-stage part refers to offered generation cost at the base case (or normal condition), (i.e. $C_g P_g^0$). Besides, the second-stage part mentions the cost of power adjustments (i.e. $C_g^s(\underline{\Delta} P_g^s + \bar{\Delta} P_g^s)$) that ensures a secure operation in the stressed condition. Indeed, the stressed condition represents theup and down power adjustments of thermal units to handle the energy imbalance owing to the stressed loading condition through a unit/line outage in real-time condition. Subsequently, the first-stage constraints are:

$$P_g^{\min} \le P_g^0 \le P_g^{\max}, \quad \forall g \tag{4b}$$

$$Q_g^{\min} \le Q_g^0 \le Q_g^{\max}, \quad \forall g \tag{4c}$$

$$\sum_{g \in \chi_n} P_g^0 + \sum_{m \in \Omega_n} P_{nm}^0 = PD_n, \quad \forall n, k \in (n, m) \tag{4d}$$

$$\sum_{g \in \chi_n} Q_g^0 + \sum_{m \in \Omega_n} Q_{nm}^0 + Q_n^{\mathrm{SVC}} = QD_n = PD_n \tan(\psi_{D_n}), \quad \forall n, k \in (n, m) \tag{4e}$$

$$\left(P_{nm}^0\right)^2 + \left(Q_{nm}^0\right)^2 \le \left(S_k^{\max}\right)^2, \quad \forall k \in (n, m) \tag{4f}$$

$$V_n^{\min} \le V_n \le V_n^{\max}, \quad \forall n \tag{4g}$$

$$(1\mathrm{i}) - (1\mathrm{j}),\ (2\mathrm{f}) - (2\mathrm{i}),\ (2\mathrm{n}) - (2\mathrm{q}),\ (3\mathrm{e}), (3\mathrm{g}) \tag{4h}$$

Constraints (4b) and (4c) force the limits of active and reactive power generation for thermal units, respectively. Constraints (4d) and (4e) denote the linearised active/reactive power balance at normal condition at each bus. In constraint (4f), since P_{nm}^0 and Q_{nm}^0 are linearised, the MVA limit for line k can be written as a second-order cone constraint. Notice that (4f) is still convex equation and can be handled by most commercial linear solvers such as Gurobi [25]. Nevertheless, if a solver requires the constraint to be strictly linear, a piecewise linearised version for (4f) can also be derived [12]. Constraint (4h) corresponds to power flow equations related to transmission lines and buses that host TCSC and SVC devices, respectively.

The second-stage constraints are:

$$P_g^s = U_g(P_g^0 + \bar{\Delta} P_g^s - \underline{\Delta} P_g^s), \quad \forall g \tag{5a}$$

$$Q_g^{\min} U_g \le Q_g^s \le Q_g^{\max} U_g, \quad \forall g \tag{5b}$$

$$\sum_{g \in \chi_n} P_g^s + \sum_{m \in \Omega_n} P_{nm}^s U_k = (1 + \lambda) PD_n, \quad \forall n, k \in (n, m) \tag{5c}$$

$$\sum_{g \in \chi_n} Q_g^s + \sum_{m \in \Omega_n} Q_{nm}^s U_k + Q_n^{\mathrm{SVC}^s} = (1 + \lambda) PD_n \cdot \tan(\psi_{D_n}), \quad \forall n, k \in (n, m) \tag{5d}$$

$$\left(P_{nm}^s U_k\right)^2 + \left(Q_{nm}^s U_k\right)^2 \le \left(S_k^{\max} U_k\right)^2, \quad \forall k \in (n, m) \tag{5e}$$

$$V_n^{\min} \le V_n^s \le V_n^{\max}, \quad \forall n \tag{5f}$$

$$(1\mathrm{i}) - (1\mathrm{j}),\ (2\mathrm{f}) - (2\mathrm{i}),\ (2\mathrm{n}) - (2\mathrm{q}),\ (3\mathrm{e}), (3\mathrm{g}) \tag{5i}$$

$$\left|P_g^0 - P_g^s\right| \le \Delta R_g^{\pm}, \quad \forall g \tag{5j}$$

Constraint (5a) links between the normal and stressed conditions of thermal units to enforce corrective actions by up/down power output adjustments, i.e. $\bar{\Delta} P_g^s / \underline{\Delta} P_g^s$. Constraint (5b) is similar to (4c) but for stressed conditions. The power flow equations for the stressed loading condition are specified by (5c) and (5d). A scalar loading margin λ is an arbitrary choice to force stress on loading for each load. Constraints (5b) and (5j) have the same expressions as (4c) and (4h), respectively, where the variables P_g^0, Q_g^0, P_{nm}^0, Q_{nm}^0,

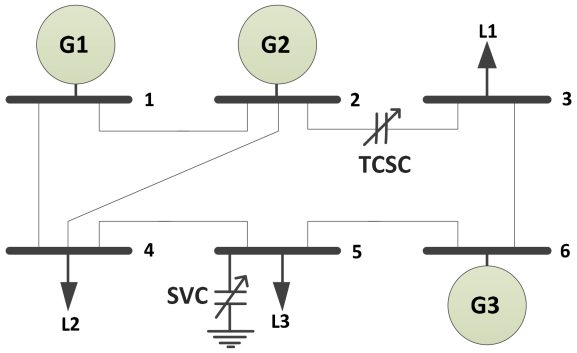

Fig. 3 *Six-bus system with the SVC and TCSC devices*

V_n^0, and Q_n^{SVC} are replaced by P_g^s, Q_g^s, P_{nm}^s, Q_{nm}^s, V_n^s, and $Q_n^{\text{SVC}^s}$, respectively. The changes in the generation of thermal units are limited by ramp constraint as mentioned in (5j). Noted that, the binary parameter U_g/U_k forces the thermal unit generation/line's power flow to be zero within (5a), (5b)/(5c), (5e) once the unit/line is in the contingency state.

The $\Delta R_g^{\pm}$ represents physically the acceptable adjustments of power output of thermal units in 10 min (i.e. 10/60 of hourly ramping of thermal units) to guarantee the desired security margin.

4 Case study

A modified six-bus system and the IEEE-118 bus system are used to analyse the proposed LAC and full AC power flow model for the OPF problem with operation of FACTS devices, i.e. the SVC and the TCSC devices. Problem for full AC power flow is a non-convex one, thus no NLP solver can generally guarantee to find the global optimum. However, using different starting points, no different solutions were found. Thus, the solutions provided in the paper are feasible for full AC power flow and appropriate from both the economical and the technical point of views. The OPF results for LAC and full AC power flow models are obtained using GAMS–CPLEX [26] and GAMS–CONOPT [27] that are suitable solvers for MILP and NLP problems, respectively. The proposed LACOPF model and full AC model were solved on an Intel *i*7, 8-core CPU at 3.40 GHz with 32 GB of RAM.

4.1 Modified six-bus system

The modified six-bus power system shown in Fig. 3 is used to illustrate the proposed framework, which has three conventional thermal units. Details of three thermal units and transmission data can be found in [28]. At the peak load, i.e. once the total load is 256 MW, the share of each load at buses 3, 4, and 5 is 84, 116, and 70 MW, respectively. In addition, when total load increases, it is distributed between these buses with the same fraction. Power flow limits of transmission lines are 30 MW for line 4–5, in order to simulate the transmission line congestion and other flow limits of transmission lines are 150 MW.

Owing to space limitations, but without loss of generality, we only show the optimal placement of FACTS devices for the TCSC and SVC devices. We do not attempt to propose a method to determine the optimal placement of FACTS devices (a technique for optimal FACTS device placement can be found in [29]). The positions of FACTS devices have been selected based on the knowledge of the network and with the aim of improving the system loadability and security.

The FACTS devices locations and data are as follows:

i. The SVC device is located at bus 5. The min and max susceptance bounds are $\underline{b} = -0.5$ p.u. and $\bar{b} = 0.5$ p.u., respectively. Besides, the number of linear blocks for linearisation of this device model is $J = 20, 30,$ and 40.
ii. The TCSC is placed on the transmission line 2–3. The min and max bounds of the reactance are $\underline{x} = -0.2$ p.u. and $\bar{x} = 0.2$ p.u., respectively. Besides, the number of linear blocks for linearisation of this device model is $I = 20, 30,$ and 40.

The following three case studies are analysed:

Case 1: comparison of the LACOPF and full ACOPF model with (without) FACTS devices models, i.e. the TCSC and SVC devices models.
Case 2: effect of FACTS devices on system loadability and security under stressed loading condition.
Case 3: case 2 under contingency state.

Case 1: this case evaluates the accuracy of the OPF solution obtained from the LACOPF modelling comparison with the solutions achieved from full ACOPF model with the FACTS devices in which stressed loading condition is considered for case 2. Also, this case is studied under both stressed loading condition and contingency state for case 3. For the six-bus system, running full ACOPF (with and without FACTS devices) with CONOPT under GAMS will lead to a feasible solution and serves as a base case of the study. Active power generations (APGs) for three thermal units and active power flow (APF) through lines 2–3 and 4–5 are shown in Tables 3 and 4, respectively. Now, the LACOPF problem with LFACTS device is solved using the proposed full MILP model. The number of linear blocks to represent the active and reactive power flow in LACOPF model is 4, 6, and 8, respectively (i.e. $L = 4$, 6, and 8). Similarly, the number of linear blocks for representing linear model (LM) of SVC and TCSC devices, in LACOPF model, is 20, 30, and 40, respectively [i.e. I (for SVC) and J (for TCSC) = 20, 30, and 40]. The accuracy of the linear formulations of TCSC and SVC has been shown in Table 5. As it can be seen, the obtained results in Tables 3 and 5, by comparing the solution results of the full ACOPF with the LACOPF model, the effectiveness and precision of the proposed model can be proved. On the other hand, as can be seen in these tables, for LACOPF with LFACTS devices model, it can be inferred that the accuracy of the results improves as the number of linear blocks increases. Among all the LACOPF with LFACTS devices modelling approaches listed in Tables 3 and 5, the LACOPF with $L = 8$ and the LFACTS devices with $I = 40$ (for TCSC) and $J = 40$ (for SVC) are the most accurate and accordingly, they are selected for the basis of the reminder study. One of the disadvantages of the LACOPF with $L = 8$ (or 4 and 6) considering the LFACTS devices is execution time, which is not reasonable for this test system. As it can be seen in Table 3, the time it takes to reach the optimal solution will be increased significantly as the number of linear blocks increases. For this reason, to overcome the above-mentioned challenges in this paper, the RM approach is proposed for the LACOPF model to solve this issue as explained in Section 2. The RM decreases the number of variables, including binary or continuous variables, as well as the number of equations which will decrease execution time significantly. Accordingly, the RM approach is considered as the best trade-off between model accuracy and solution time. For example, in Table 3, for the LACOPF without LFACTS devices model, the RM approach reduces the solution time by ∼98%, but the approximation error for the APGs for three thermal units is <0.005. Also, the LACOPF model with $L = 4$ and $L = 6$ reduce the solution time by ∼83 and 53%, respectively, and creates only <0.002 MW absolute error for APG for three thermal units. Similarly, the results for the APF from the LACOPF/the full ACOPF with (without) LFACTS/ FACTS devices, through lines 2–3 and 4–5 obtained from the RM and $L = 4$ and $L = 6$, are given in Table 4. As it can be seen, the results for the RM approach will be approximately the same. Besides, as shown in Table 5, the accuracy of LMs of the SVC and TCSC devices are increasing as the number of linear blocks increases, i.e. increase I (for SVC) and J (for TCSC). As shown in Table 5, the LM of the SVC and TCSC with $I = 40$ and $J = 40$ have the most accuracy in the LACOPF model for both cases 2 and 3. For instance, as can be seen in the last row of this table, the optimal setting of the SVC and TCSC devices in case 2 for the full ACOPF model are 0.377 and 0.132 p.u., respectively. Also in the LACOPF model, the optimal setting of the SVC and TCSC with [$L = 8$, $I = 40$, $J = 40$] and the RM approach with [$I = 40$, $J = 40$] are 0.366 and 0.130 p.u., respectively. As can be seen in the obtained results from the LACOPF model and full ACOPF model, the approximation error

for optimal setting of these devices are 0.011 and 0.002, respectively. This simple comparison clearly shows that the proposed method for linearising the SVC and TCSC devices models is so effective and accurate and the results will be verifiable and promising.

Case 2: in this case, the OPF problem with (without) FACTS devices is certainly feasible for $\lambda = 0$. However, as the loading parameter λ increases, the OPF problem may become infeasible because the desired value of λ cannot be satisfied. Nevertheless, since the loading parameter is increased at each step by 0.1%, if the solution is infeasible at a specified step, say $i + 1$, is the maximum loading condition with an error <0.1%. Simulations results are depicted in Table 6. Table 6 represents the objective function TC, namely the total cost of OPF problem, as a function of the loading parameter λ. As can be seen in Table 6, for $\lambda > 1.129$, the OPF problem for the test system without FACTS devices becomes infeasible. By analysing the selected SVC or/and TCSC devices and the corresponding results in Table 6, we can better know the effect of each device on the test system. For example, for $1.130 \leq \lambda \leq 1.188$, the security constraints have limits on lines and voltage limits (in particular, on line 4–5 and at bus 3). As shown in Table 6, the SVC device by controlling voltage levels can increase values of the $\lambda^{\max}$ or improve the maximum system loadability (MSL). Nevertheless, the effects of this device on power flow through transmission lines are negligible, which is reasonable, since this device control voltage levels. For $\lambda > 1.188$, the security constraints have limits on power flowing through lines (in particular, through line 4–5). As can be seen in Table 6, the most effective FACTS devices on the MSL is in the case of using TCSC, that is to expectable because this device can control lines power flow. For $\lambda > 1.188$, the effects of the SVC device are negligible because there is not only voltage issue in test system. As it has been discussed above, the influences of the SVC (voltage controlling device) are mostly independent from the influences of the TCSC (transmission line power flow controlling device). This fact proposes that the simultaneous utilisation of one voltage controlling and a power flow controlling devices can lead to more increase in MSL (i.e. the $\lambda^{\max}$ is 1.336), than using each of them individually. This is confirmed in Table 6. Besides, as shown in Table 6, the TC is increased by further improve in MSL, which is reasonable, since this action rise total generation level and thermal units redispatching to sustaining load generation balance.

LFACTS devices model, the RM approach reduces the solution time by ∼98%, but the approximation error for the APGs for three thermal units is <0.005. Also, the LACOPF model with $L = 4$ and $L = 6$ reduce the solution time by ∼83 and 53%, respectively, and creates only <0.002 MW absolute error for APG for three thermal units. Similarly, the results for the APF from the LACOPF/the full ACOPF with (without) LFACTS/ FACTS devices, through lines 2–3 and 4–5 obtained from the RM and $L = 4$ and $L = 6$, are given in Table 4. As it can be seen, the results for the RM approach will be approximately the same. Besides, as shown in Table 5, the accuracy of LMs of the SVC and TCSC devices are increasing as the number of linear blocks increases, i.e. increase I (for SVC) and J (for TCSC). As shown in Table 5, the LM of the SVC and TCSC with $I = 40$ and $J = 40$ have the most accuracy in the LACOPF model for both cases 2 and 3. For instance, as can be seen in the last row of this table, the optimal setting of the SVC and TCSC devices in case 2 for the full ACOPF model are 0.377 and 0.132 p.u., respectively. Also in the LACOPF model, the optimal setting of the SVC and TCSC with [$L = 8$, $I = 40$, $J = 40$] and the RM approach with [$I = 40$, $J = 40$] are 0.366 and 0.130 p.u., respectively. As can be seen in the obtained results from LACOPF model and full ACOPF model, the approximation error for optimal setting of these devices are 0.011 and 0.002, respectively. This simple comparison clearly shows that the proposed method for linearising the SVC and TCSC devices models is so effective and accurate and the results will be verifiable and promising.

Also, the results contained in Table 6 compare the accuracy of the MSL obtained from the MILP formulation and the number of linear blocks used for the LACOPF model, while optimal settings of the linear SVC and TCSC devices are [$L = 8$, $I = 40$, $J = 40$] and for the RM approach are [$I = 40$, $J = 40$]. As can be seen in Table 6, the MSL obtained from full MILP formulation, with [$L = 8$, $I = 40$, $J = 40$], and the RM approach are 1.130 and 1.129, respectively. Among the both MILP modelling approaches listed in this table, the full MILP formulation, with [$L = 8$, $I = 40$, $J = 40$], is the most accurate with a highest solution time. The RM approach relaxes constraint (2p) for prioritising the lower linear blocks. This approach reduces the solution time by ∼98.33%, i.e. from (60–1 s as can be seen in Table 4), and the maximum error is 0.18%, while for full MILP formulation is 0.088%. The study results show that the RM approach is better while it makes the best trade-off between model accuracy and solution time.

Case 3: in this case, the outage of line 2–4 is considered as a stressed condition. This is the worst contingency for the six-bus test system. The outage of this line causes congestions in transmission lines, i.e. line 2–3, and voltage drop at the test system buses, i.e. at bus 5. In this condition, we increase loading parameter

Table 3 Accuracy of the LACOPF model: the APG of three thermal units

FACTS device		OPF model	Case 2			Case 3			Time, s
			G1	G2	G3	G1	G2	G3	
no. of device	LAC	RM	0.449	1.872	0.390	Inf	Inf	Inf	<1
		$L = 4$	0.451	1.877	0.400	Inf	Inf	Inf	10
		$L = 6$	0.452	1.875	0.390	Inf	Inf	Inf	25
		$L = 8$	0.452	1.876	0.400	Inf	Inf	Inf	60
		AC	0.452	1.876	0.400	Inf	Inf	Inf	<1
SVC	LAC	RM, $I = 40$	0.353	1.948	0.428	1.387	1.186	0.179	<2
		$L = 4$, $I = 20$	0.351	1.951	0.426	1.386	1.184	0.185	12
		$L = 6$, $I = 30$	0.351	1.951	0.428	1.387	1.185	0.180	31
		$L = 8$, $I = 40$	0.352	1.951	0.427	1.388	1.187	0.179	71
		AC	0.352	1.951	0.428	1.389	1.187	0.179	<2
TCSC	LAC	RM, $J = 40$	1.451	0.960	0.349	2.085	0.298	0.373	<2
		$L = 4$, $J = 20$	1.452	0.958	0.349	2.087	0.292	0.375	14
		$L = 6$, $J = 30$	1.453	0.958	0.351	2.083	0.295	0.374	34
		$L = 8$, $J = 40$	1.453	0.960	0.350	2.082	0.298	0.372	74
		AC	1.453	0.961	0.350	2.084	0.298	0.372	<2
SVC and TCSC	LAC	RM, $J = 40$, $I = 40$	1.503	0.947	0.321	1.878	0.363	0.500	<2
		$L = 4$, $J = 20$, $I = 20$	1.502	0.941	0.321	1.878	0.366	0.480	17
		$L = 6$, $J = 30$, $I = 30$	1.501	0.948	0.321	1.877	0.365	0.500	39
		$L = 8$, $J = 40$, $I = 40$	1.500	0.948	0.320	1.878	0.363	0.500	88
		AC	1.501	0.948	0.320	1.879	0.364	0.500	<2

λ step by step, each step is 0.1%, until the OPF problem becomes infeasible. As shown in Tables 3, 4, and 6, in case 3, the OPF problem without any FACTS devices cannot satisfy the AC network security constraints; as a result, the OPF problem becomes infeasible (Inf). The outage of line 2–4, besides, leads to congestion and consequently shortage in the reactive power injection at bus 5. Accordingly, at this condition, the voltage drop issue happens at this bus. The SVC device, which is installed at bus 5, has been solved the voltage drop issue by increasing the injection of reactive power at this bus and keeping the steady-state voltage of this bus in the acceptable range. For this reason, as can be seen in Table 5, by comparison of this case with case 2, the B_n^{SVC} value is increased from $B_n^{\mathrm{SVC}} = -0.196$ p.u. (in case 2) to $B_n^{\mathrm{SVC}} = -0.500$ p.u. (in case 3), it shows increase in the injection of reactive power. The MSL, i.e. $\lambda^{\max}$, for the OPF problem with the SVC device is 1.00 p.u. As shown in Table 4, in case 3, power flowing through line 2–3, i.e. 1.498 p.u., is very close to its capacity limit, i.e. 1.50 p.u., which is the most important obstacle to increase the MSL. In order to lower the power flowing on this line, we implement the TCSC device. As shown in Table 4, the power flowing through line 2–3 is decreased from 1.498 to 1.471 p.u. by implementing the TCSC device. This action caused to improve the MSL by 3.8% (improved from 1.00 to 1.04, as

Table 4 Accuracy of the LACOPF model: the APF of lines 2–3 and 4–5, with (without) the LFACTS/FACTS devices

Device	Line	Linear block (for LACOPF)	Case 2		Case 3	
			LACOPF	ACOPF	LACOPF	ACOPF
no. of device	2–3	RM	0.985	0.992	Inf	Inf
		$L = 4$	0.981			
		$L = 6$	1.000			
		$L = 8$	0.989			
	4–5	RM	0.278	0.280	Inf	Inf
		$L = 4$	0.283			
		$L = 6$	0.285			
		$L = 8$	0.281			
SVC	2–3	RM, $J = 40$	0.995	0.999	1.500	1.498
		$L = 4$, $J = 20$	0.998		1.497	
		$L = 6$, $J = 30$	1.000		1.497	
		$L = 8$, $J = 40$	1.000		1.498	
	4–5	RM, $J = 40$	0.280	0.300	0.022	0.023
		$L = 4$, $J = 20$	0.290		0.024	
		$L = 6$, $J = 30$	0.300		0.023	
		$L = 8$, $J = 40$	0.300		0.023	
TCSC	2–3	RM, $I = 40$	1.270	1.300	1.468	1.471
		$L = 4$, $I = 20$	1.290		1.470	
		$L = 6$, $I = 30$	1.300		1.471	
		$L = 8$, $I = 40$	1.300		1.471	
	4–5	RM, $J = 40$	0.259	0.263	0.129	0.131
		$L = 4$, $J = 20$	0.261		0.132	
		$L = 6$, $J = 30$	0.264		0.131	
		$L = 8$, $J = 40$	0.263		0.131	
SVC and TCSC	2–3	RM, $I = 40$, $J = 40$	1.483	1.488	1.173	1.179
		$L = 4$, $I = 20$, $J = 40$	1.488		1.180	
		$L = 6$, $I = 30$, $J = 40$	1.488		1.181	
		$L = 8$, $I = 40$, $J = 40$	1.488		1.179	
	4–5	RM, $I = 40$, $J = 40$	0.294	0.295	0.146	0.150
		$L = 4$, $I = 20$, $J = 40$	0.292		0.148	
		$L = 6$, $I = 30$, $J = 40$	0.295		0.150	
		$L = 8$, $I = 40$, $J = 40$	0.295		0.150	

Table 5 Accuracy of the LFACTS device models: the SVC and TCSC models

Device	Linear block (for LACOPF)	Case 2		Case 3	
		LAC OPF	AC OPF	LAC OPF	AC OPF
SVC	$L = 4$, $I = 20$	−0.200	−0.196	−0.500	−0.500
	$L = 8$, $I = 30$	−0.200		−0.500	
	$L = 10$, $I = 40$	−0.197		−0.500	
	RM, $I = 40$	−0.195		−0.500	
TCSC	$L = 4$, $J = 20$	−0.100	−0.094	−0.100	−0.100
	$L = 8$, $J = 30$	−0.090		−0.100	
	$L = 10$, $J = 40$	−0.094		−0.100	
	RM, $J = 40$	−0.095		−0.100	
SVC and TCSC	$L = 4$, $J = 20$, $I = 20$	−0.400/−0.130	−0.377/−0.132	−0.500/−0.070	−0.500/−0.069
	$L = 8$, $J = 30$, $I = 30$	−0.350/−0.133		−0.500/−0.070	
	$L = 10$, $J = 40$, $I = 40$	−0.366/−0.130		−0.500/−0.067	
	RM, $J = 40$, $I = 40$	−0.366/−0.130		−0.500/−0.070	

observed in Table 5). It can be inferred from Table 5, the SVC and TCSC devices cannot improve the MSL significantly. However, in the case of simultaneous implementation of the SVC and TCSC devices, there is a significant decrease in power flowing through line 2–3 by TCSC device (i.e. >21%), and more increase in reactive power injection at bus 5 resulting in voltage improvement at this bus by SVC device. This fact is shown in Table 5 by increasing the B_n^{SVC} value. Finally, in the case of concurrent operation of SVC and TCSC, the MSL is improved by 10 and 6.4% with respect to using individual SVC or TCSC, respectively.

4.2 Modified IEEE 118-bus system

The modified IEEE 118-bus system has 54 thermal units, 186 lines, and 91 load buses. The parameters of transmission network, load profiles, and thermal units are given in motor.ece.iit.edu/data/SCUC_118. The peak load is 7306 MW. Also in this test system, the line limits for a few transmission lines are reduced to 100 MW in order to simulate the transmission system congestion. The FACTS devices are located in their corresponding optimal locations in the modified IEEE 118-bus test system. Hence, all the FACTS devices are located independently at a single location and its impact on the MSL is investigated [29].

Based on load flow analysis, the heavily loaded lines with low capacity in the modified IEEE 118-bus system are lines [11 (buses 5–11), 55 (buses 39–40), 70 (buses 49–50), 136 (buses 85–89), and 168 (buses 104–105)] where the series devices TCSC are located. The limitation of the effective reactance of each TCSC device is set to 90% capacitive and 40% inductive of the original reactance of the transmission line where the TCSC device is located. Also, the buses that need more reactive power compensation are buses 7, 69, 77, 49, 34, and 106 where the shunt devices SVC are located. The min and max susceptance bounds for each SVC devices are similar to the previous test system. Four cases are considered here, that cases 1–3 are similar to cases 1–3 of the previous test system.

Case 1: the simulations are performed to obtain the APF and the APG using the LACOPF model and the full ACOPF model. Furthermore, we consider the SVC and TCSC devices simultaneously in both the OPF models. The number of linear blocks for representing the active and reactive power flow in LACOPF model is 4, which is named LM here, is considered for the modified IEEE 118-bus system. Similarly, the number of linear blocks to represent the LM of the SVC and the TCSC devices for both models mentioned for the LACOPF model, i.e. the LM and the RM models, is I and $J = 30$.

Considering the full ACOPF results as the reference, the calculation errors are given by:

$$\Delta_{nm}^{\mathrm{LAC}} = \left| P_{nm}^{\mathrm{AC}} - P_{nm}^{\mathrm{LAC}} \right| \tag{6a}$$

$$\Delta_{g}^{\mathrm{LAC}} = \left| P_{g}^{\mathrm{AC}} - P_{g}^{\mathrm{LAC}} \right| \tag{6b}$$

Equation (6a) is the calculation error of the APF in line (n, m) which are obtained from both models of the LACOPF, i.e. the LM and RM, and the full ACOPF solution, respectively. Also, (6b) is the calculation error of the APG from thermal unit g similar to (6a). As can be seen in Fig. 4, the maximum value of the error calculated for $\Delta_{nm}^{\mathrm{LAC}}$, for the LM and RM models, are 0.0092 and 0.0252 p.u., respectively. Also, the mean value of error calculated for $\Delta_{nm}^{\mathrm{LAC}}$, for these models are 0.018 and 0.052 p.u., respectively. Similarly, in Fig. 5, the maximum $\Delta_{g}^{\mathrm{LAC}}$ value for the LM and RM models are 0.017 and 0.0477 p.u., respectively. In addition, the mean value of $\Delta_{g}^{\mathrm{LAC}}$ for these models is 0.0012 and 0.00617 p.u., respectively. These results indicate that the APF through the lines and the APG of thermal units obtained by the proposed LACOPF model provide more precise for large-scale systems. The elapsed time to solve the LACOPF problem by the LM approach is about >700 s and by the RM approach is about <10 s. These results indicate the accuracy of RPF and RPG for the LM approach, which is calculated by the LACOPF model, is increased on large-scale system. However, this should be taken into account that with the LM approach, the solution time is increased. The results show that the RM approach has the best trade-off between model accuracy and solution time for the large-scale systems.

Also, in this case, the $\lambda^{\max}$ and the TC obtained from the full ACOPF model with (without) FACTS devices are given in Table 7. The same results are approximately obtained by the proposed method using the LACOPF with (without) LFACTS devices. Noted that, the LACOPF model in Table 7 is modelled by the RM approach. For this approach, the $\lambda^{\max}$ and the TC are given in Table 7 and the written program has 84,353 single equations, 96,630 single variables, and 1116 binary variables. As it can be seen in Table 7, the calculation error of the obtained results from the LACOPF model (modelled by RM) and the ACOPF model are very small, i.e. for the $\lambda^{\max}$ and TC are <0.005, which is a very worthy precise. The elapsed time to solve the OPF problem with (without) FACTS devices by the full ACOPF approach is ∼20 s and by LACOPF (by RM method) approach is <10 s. Finally, as the results show, the LACOPF that is modelled by the RM method is completely accepted from our OPF problem with (without) FACTS devices and has a reasonable run time.

Case 2: this case is similar to case 2 in the previous test system. Therefore, as can be seen in Table 7, the OPF problem is feasible for no FACTS devices and the value of $\lambda^{\max}$ is 1.208. Note, this value, $\lambda^{\max} = 1.208$, is served as reference for the MSL. In this case, the loading parameter is increased similar to the previous test system and maximum loading condition is obtained. Simulations

Table 6 MSL and the TC for the six-bus system for cases 2 and 3

Device		Linear block (for LACOPF)	LACOPF		ACOPF	
			$\lambda^{\max}$	TC	$\lambda^{\max}$	TC
case 2	no. of device	$L = 8$	1.130	7518.126	1.131	7520.896
		RM	1.129	7515.086		
	SVC	$L = 8$, $I = 40$	1.189	7856.382	1.191	7861.432
		RM, $I = 40$	1.188	7853.432		
	TCSC	$L = 8$, $J = 40$	1.336	8412.120	1.337	8418.897
		RM, $J = 40$	1.334	8407.170		
	SVC and TCSC	$L = 8$, $J = 40$, $I = 40$	1.338	8378.134	1.338	8379.875
		RM, $J = 40$, $I = 40$	1.336	8370.775		
case 3	no. of device	$L = 8$	Inf	Inf	Inf	Inf
		RM	Inf	Inf		
	SVC	$L = 10$, $I = 40$	1.000	6139.340	1.000	6141.780
		RM, $I = 40$	1.000	6135.600		
	TCSC	$L = 10$, $J = 40$	1.045	6389.125	1.050	6392.160
		RM, $J = 40$	1.040	6388.270		
	SVC and TCSC	$L = 10$, $J = 40$, $I = 40$	1.107	6985.676	1.109	6992.175
		RM, $J = 40$, $I = 40$	1.112	6986.135		

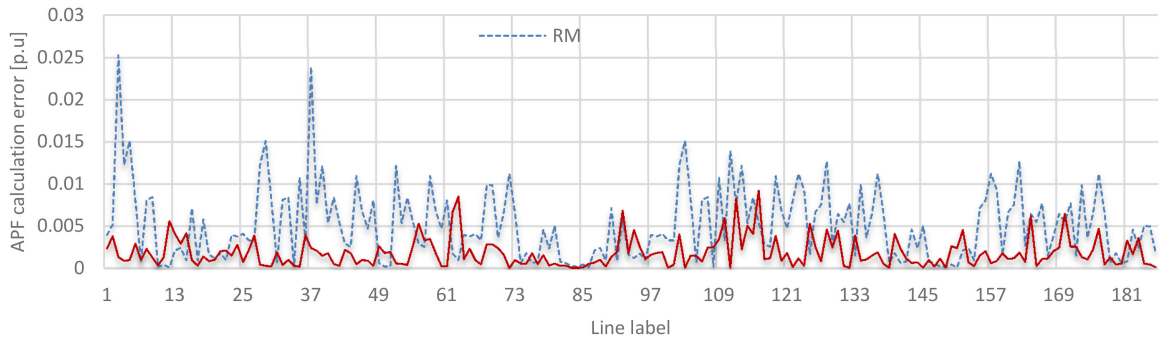

Fig. 4 *APF calculation error for the IEEE 118-bus system for LACOPF modelled by the LM and the RM approaches*

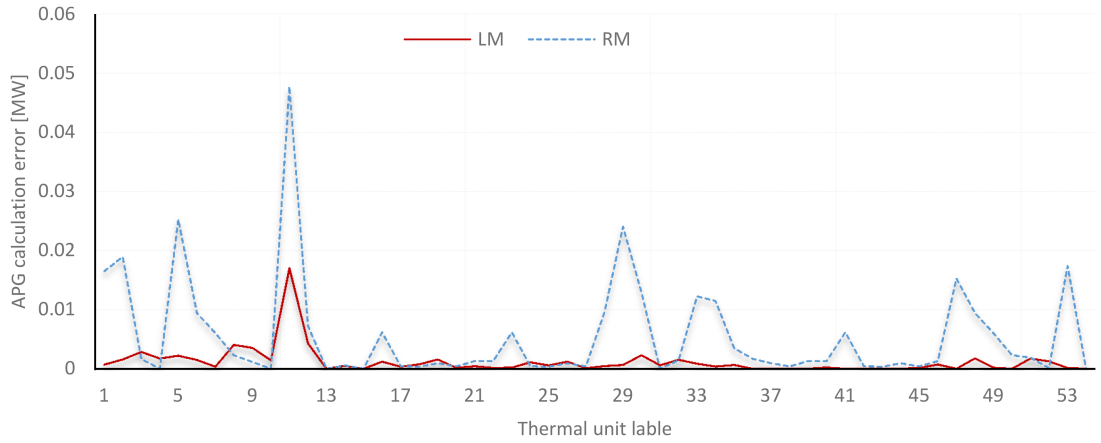

Fig. 5 *APG calculation error for the IEEE 118-bus system for LACOPF modelled by the LM and the RM approaches*

Table 7 MSL and TC for the IEEE 118-bus system for cases 2 and 3

Device		LACOPF		ACOPF	
		λ^{max}	TC	λ^{max}	TC
case 2	no. of device	1.212	165,889.152	1.208	165,371.231
	SVC	1.301	181,319.669	1.298	179,057.655
	TCSC	1.454	208,232.502	1.451	207,699.471
	SVC and TCSC	1.533	222,347.340	1.529	221,628.968
case 3	no. of device	Inf	Inf	Inf	Inf
	SVC	1.044	159,340.413	1.042	158,824.548
	TCSC	1.151	169,172.709	1.153	168,653.863
	SVC and TCSC	1.251	190,053.951	1.244	189,528.350

results are illustrated in Table 7. This table represents the TC and the MSL. As can be seen from this table, if we compare the TCSC and SVC for the modified 118-bus network, we see that by using the TCSC device, we have ∼16.70% loadability improvement while with the SVC, the rate is ∼7%. Comparing the results for TCSC and SVC devices, it can be inferred that the TCSC device would be more effective than the SVC in improving the MSL. Finally, we have the most improve MSL, for modified 118-bus test system, once that the TCSC and SVC devices are considered simultaneously. In this situation, as it clear from Table 7, we have ∼21% improvement in the MSL.

Case 3: this case is similar to case 3 in the previous test system. Here, three simultaneous contingencies are considered. The contingencies include outages of thermal unit 28, transmission lines 75–77, and 85–89. The first OPF problem is feasible for the outage of transmission line 75–77. Therefore, the contingency of transmission line 75–77 is controllable without FACTS devices. Since the OPF solution cannot lead to a feasible solution for the outages of unit 28 and transmission line 85–89, these contingencies are uncontrollable without FACTS devices. The value of λ^{max}, for the OPF problem with the SVC device, is 1.042. Also, we have ∼10% improvement in the MSL with the TCSC device. The results of concurrent operation of the SVC and TCSC devices are presented in Table 7, which show ∼16.23% improvement in the MSL. Finally, the simulation results in this table show that the concurrent operation of these devices have the most efficiency in increasing the MSL under contingency state.

Case 4: in this case, the effect of the number of FACTS devices (TCSC and SVC) on the number of congested lines has been studied. As can be seen in Fig. 6, the number of congested transmission lines is reduced by increasing the number of TCSCs and SVCs from 1 to 5 and 1 to 6, respectively, in the test system. Figs. 3*a* and *b* show how the congestion of transmission lines decreases as more FACTS devices are allowed to be used. This figure shows that the congestion reduction in transmission lines is more significant for the first few FACTS (especially for the TCSC devices) and then the congestion curves are going to be saturated. On the other hand, as shown in Figs. 3*a* and *b*, the TCSC is more effective on congestion reduction in transmission lines than the SVC. For this reason, the voltage support provided by the SVC does not reduce the number of congested lines. Nonetheless, the TCSC is able to reduce the number of congested lines since it decrease the series impedance of the congested transmission lines, hence allows reducing congestion of transmission lines. For the IEEE 118-bus system, the binding constraints are mainly the limits on transmission lines. As expected, the effective FACTS devices among TCSC and SVC on the number of congested lines are the TCSC device because this device has better control on line power

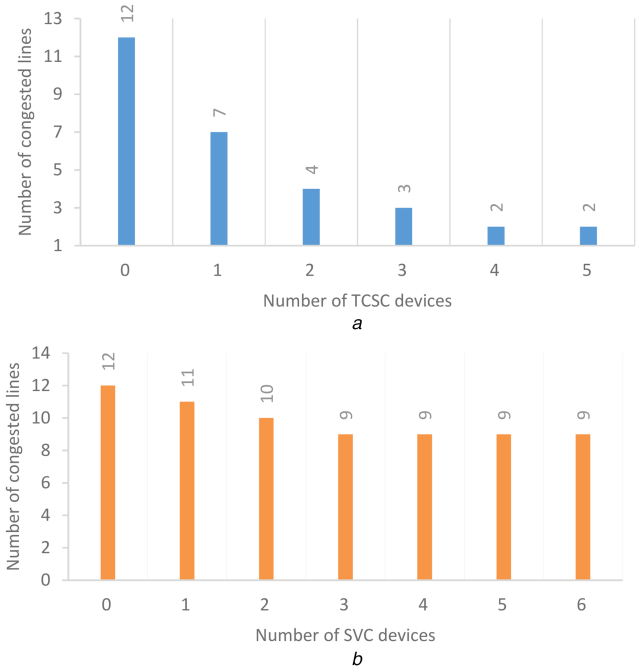

Fig. 6 *Number of congested lines versus*
(a) Number of TCSC devices, ***(b)*** Number of SVC devices in the IEEE-118 bus system

flows. For this test system, the effects of the SVC are negligible because there is no voltage problem. Accordingly, as shown in Fig. 6*a*, the number of this device has a small effect on the congested lines. However, when the number of TCSC and SVC devices is increased, from 1 up to 5, the number of congested lines has not changed. This is basically due to the fact that the TCSC and SVC devices reach their control limits.

5 Conclusions

This paper provides a methodology to maximise system loadability and system security using an OPF with FACTS devices. The OPF problem presented in this paper is based on a new LACOPF model with linearised FACTS devices model. Among FACTS devices, SVC and TCSC are selected for this study. The proposed LACOPF and LFACTS models approximate the full AC network constraints and the non-linear nature of the SVC and TCSC devices more accurately, and therefore provide more realistic operation solutions. The paper shows that full ACOPF with SVC and TCSC devices is an NLP problem that is transformed into an MILP by the proposed method. Therefore, the LACOPF problem with LFACTS devices can be solved by available efficient commercial-grade software. Since this paper reformulated the problem as an MILP, the global optimal solution of the approximated model is guaranteed to be found as revealed in the simulation results. The simulation results on the modified IEEE-118 bus system show that the proposed LACOPF model can be applied to solve OPF problems with LFACTS devices, to more accurately approximate the AC network with FACTS devices compared to a DCOPF model.

6 References

[1] Lehmkoster, C.: 'Security constrained optimal power flow for an economical operation of FACTS-devices in liberalized energy markets', *IEEE Trans. Power Deliv.*, 2002, **17**, pp. 603–608

[2] Bertsekas, D. P.: '*Nonlinear programming*' (Athena Scientific Belmont, Nashua, NH, USA, 1999)

[3] Mukherjee, A., Mukherjee, V.: 'Solution of optimal power flow with FACTS devices using a novel oppositional krill herd algorithm', *Int. J. Electr. Power Energy Syst.*, 2016, **78**, pp. 700–714

[4] Nireekshana, T., Rao, G. K., Raju, S. S. N.: 'Enhancement of ATC with FACTS devices using real-code genetic algorithm', *Int. J. Electr. Power Energy Syst.*, 2012, **43**, pp. 1276–1284

[5] Pillay, A., Karthikeyan, S. P., Kothari, D.: 'Congestion management in power systems – a review', *Int. J. Electr. Power Energy Syst.*, 2015, **70**, pp. 83–90

[6] Berizzi, A., Delfanti, M., Marannino, P., *et al.*: 'Enhanced security-constrained OPF with FACTS devices', *IEEE Trans. Power Syst.*, 2005, **20**, pp. 1597–1605

[7] Gasperic, S., Mihalic, R.: 'The impact of serial controllable FACTS devices on voltage stability', *Int. J. Electr. Power Energy Syst.*, 2015, **64**, pp. 1040–1048

[8] Ghahremani, E., Kamwa, I.: 'Optimal placement of multiple-type FACTS devices to maximize power system loadability using a generic graphical user interface', *IEEE Trans. Power Syst.*, 2013, **28**, pp. 764–778

[9] Sahraei-Ardakani, M., Hedman, K.W.: 'A fast LP approach for enhanced utilization of variable impedance based FACTS devices', *IEEE Trans. Power Syst.*, 2016, **31**, pp. 2204–2213

[10] Sahraei-Ardakani, M., Hedman, K. W.: 'Day-ahead corrective adjustment of FACTS reactance: a linear programming approach', *IEEE Trans. Power Syst.*, 2016, **31**, pp. 2867–2875

[11] Zarate-Minano, R., Conejo, A., Milano, F.: 'OPF-based security redispatching including FACTS devices', *IET Gener. Transm. Distrib.*, 2008, **2**, pp. 821–833

[12] Akbari, T., Bina, M. T.: 'Linear approximated formulation of AC optimal power flow using binary discretisation', *IET Gener. Transm. Distrib.*, 2016, **10**, pp. 1117–1123

[13] Nasri, A., Conejo, A. J., Kazempour, S. J., *et al.*: 'Minimizing wind power spillage using an OPF with FACTS devices', *IEEE Trans. Power Syst.*, 2014, **29**, pp. 2150–2159

[14] Henneaux, P., Kirschen, D. S.: 'Probabilistic security analysis of optimal transmission switching', *IEEE Trans. Power Syst.*, 2016, **31**, pp. 508–517

[15] Nagalakshmi, S., Kamaraj, N.: 'On-line evaluation of loadability limit for pool model with TCSC using back propagation neural network', *Int. J. Electr. Power Energy Syst.*, 2013, **47**, pp. 52–60

[16] Zhang, H., Heydt, G. T., Vittal, V., *et al.*: 'An improved network model for transmission expansion planning considering reactive power and network losses', *IEEE Trans. Power Syst.*, 2013, **28**, pp. 3471–3479

[17] Jordehi, A. R.: 'Particle swarm optimisation (PSO) for allocation of FACTS devices in electric transmission systems: a review', *Renew. Sust. Energy Rev.*, 2015, **52**, pp. 1260–1267

[18] Ongsakul, W., Bhasaputra, P.: 'Optimal power flow with FACTS devices by hybrid TS/SA approach', *Int. J. Electr. Power Energy Syst.*, 2002, **24**, pp. 851–857

[19] Khorsandi, A., Hosseinian, S., Ghazanfari, A.: 'Modified artificial bee colony algorithm based on fuzzy multi-objective technique for optimal power flow problem', *Electr. Power Syst. Res.*, 2013, **95**, pp. 206–213

[20] Sahraei-Ardakani, M., Blumsack, S. A.: 'Transfer capability improvement through market-based operation of series FACTS devices', 2015

[21] Misener, R., Floudas, C.: 'Piecewise-linear approximations of multidimensional functions', *J. Optim. Theory Appl.*, 2010, **145**, pp. 120–147

[22] Beale, E., Forrest, J. J.: 'Global optimization using special ordered sets', *Math. Program.*, 1976, **10**, pp. 52–69

[23] Fuerte-Esquivel, C., Acha, E., Ambriz-Perez, H.: 'A thyristor controlled series compensator model for the power flow solution of practical power networks', *IEEE Trans. Power Syst.*, 2000, **15**, pp. 58–64

[24] Ambriz-Perez, H., Acha, E., Fuerte-Esquivel, C.: 'Advanced SVC models for Newton–Raphson load flow and Newton optimal power flow studies', *IEEE Trans. Power Syst.*, 2000, **15**, pp. 129–136

[25] Gurobi Optimization, Gurobi Optimizer Reference Manual. [Online]. Available at http://www.gurobi.com

[26] CPLEX, GAMS. The Solver Manuals. GAME/CPLEX, 1996 [Online]. Available at http://www.gams.com/

[27] Drud, A. S.: GAMS/CONOPT. ARKI consulting and development, Bagsvaerd, Denmark, 1996 [Online]. Available at http://www.gams.com/

[28] Khodaei, A., Shahidehpour, M.: 'Transmission switching in security-constrained unit commitment', *IEEE Trans. Power Syst.*, 2010, **25**, pp. 1937–1945

[29] Duong, T., JianGang, Y., Truong, V.: 'Application of min cut algorithm for optimal location of FACTS devices considering system loadability and cost of installation', *Int. J. Electr. Power Energy Syst.*, 2014, **63**, pp. 979–987